Changes of optical properties of two carbonaceous nanoparticles upon their coalescence: Computations at the atomistic level.

N. Brosseau-Habert

Institut FEMTO-ST – UMR 6274 SUPMICROTECH/Université Marie et Louis Pasteur/CNRS, Besançon, France.

Institut UTINAM - UMR 6213 Université Marie et Louis Pasteur/CNRS, Besancon, France

F. Miradji

Institut FEMTO-ST – UMR 6274 SUPMICROTECH/Université Marie et Louis Pasteur/CNRS, Besançon, France.

M. Devel

Institut FEMTO-ST – UMR 6274 SUPMICROTECH/Université Marie et Louis Pasteur/CNRS, Besançon, France.

S. Picaud

Institut UTINAM - UMR 6213 CNRS/Université Marie et Louis Pasteur, Besançon, France

Abstract

Once emitted into the atmosphere, soot nanoparticles undergo ageing processes during which they may collide and form aggregates, possibly modifying their physico-chemical properties. Here, we especially focus on their optical properties and the Dynamic Atomic Dipole Interaction (DADI) approach has been used to calculate the refractive index and the mass absorption cross section of two carbonaceous nanoparticles modeling soot. Three typical situations have been considered: separated particles, particles just in contact, interpenetrated particles. Molecular dynamics simulations based on a reactive interatomic interaction potential have been used to get the atomic coordinates in the three configurations considered and the graphite parametrization has been used for defining the polarizability tensors of the carbon atoms. The results of the DADI calculations show that the interpenetration of the nanoparticles actually modifies both their refractive index and their mass absorption cross section with respect to well-separated particles. Because the corresponding changes are shown to be tightly bound to local modifications of the close neighborhood of the carbon

 $[\]label{eq:mail_addresses:} \ \texttt{michel.devel@femto-st.fr} \ (M. \ Devel), \ \texttt{sylvain.picaud@univ-fcomte.fr} \ (S. \ Picaud)$

atoms, the present study emphasizes that an as precise as possible description of the coalescence process at the atomic scale is required to better quantify the influence of aggregation processes on the optical properties of carbonaceous nanoparticles. In addition, calculations at the atomic scale via the DADI method allow the computation of refractive indices taking into account the local modifications of the particles, which are shown to be then usable as inputs in macroscopic models, such as T-matrix. This would certainly help at better assessing, e.g., the actual impact of soot on climate.

1. Introduction

The carbonaceous fraction is an important component of atmospheric particulate matter (PM). It includes both organic and refractory light-absorbing parts [1, 2], which mainly originate from incomplete combustion processes of carbon-containing fuels as well as from biomass burning [3]. Although distinction has been made between brown (BrC) and black (BC) carbon particles as a function of their organic carbon content [4, 5], all the carbonaceous particles interact with ultraviolet and visible solar radiations, thus directly impacting on the global Earth's radiative balance [6, 7]. These particles may also act as cloud condensation nuclei or ice nuclei by trapping water molecules, thus playing an essential role in cloud formation [8], which adds to their potential impact on climate (indirect effects) [9, 10]. Thus, the carbonaceous fraction of the atmospheric PM has become an important concern for atmospheric sciences, with the evident need for a better characterization of the physicochemical properties of the corresponding particles [3].

Although BrC has recently received an increasing attention, a thorough understanding of its role in the atmosphere is far from being achieved, mainly due to the diversity of the sources, the complexity of the formation mechanisms, and the huge variety of particles that can be considered as BrC [5, 11]. On the other hand, BC appears simpler and it has been quite easily defined by its chemical, physical and spectroscopic properties [12, 13]. Indeed, BC can be viewed as nanometer-sized particles, mainly made of nearly elemental carbon with sp^2 -bonding between carbon atoms arranged in multi-layered more or less graphitized sheets forming concentric, spherical, monomers which aggregate into open, lacy structures of various fractal dimensions [12, 14]. These structures may also contain a few percent of H and O atoms, as well as C atoms with sp^3 hybridization [15]. Nevertheless, despite this narrow definition, numerous research projects are still required to elucidate the physico-chemical characteristics of BC nanoparticles and, thus, to better quantify their impact on air quality [16, 17, 18] and on climate forcing [10, 13, 19, 20, 21].

Besides experimental *in-situ* measurements of their properties [12, 14, 22], numerous efforts have been done towards an accurate modeling of the interaction of BC with UV-Visible-IR radiation [23]. From a theoretical point of view, absorption and scattering properties of BC can be computed analytically if the dielectric constant or refractive index is accurately known [13, 24], by using Lorenz-Mie theory and/or the Rayleigh-Debye-Gans theory for Frac-

tal Aggregates, and provided that some assumptions are made on the shape, the size and the chemical composition of these combustion-emitted particles [25, 26, 27]. Powerful numerical approaches such as the T-matrix [28, 29, 30] or the Discrete Dipole Approximation (DDA) [31, 32] methods can also be used for quantifying absorption and scattering of radiation by BC particles of arbitrary shape and by periodic structures [23]. However, despite of their strong theoretical basis, all these methods have been shown to underpredict the measured mass absorption cross section (MAC) of BC, a failure which has been attributed to the use of an inaccurate refractive index, although other possible biases in these models have not been completely ruled out [13]. The uncertainty concerning the values that must be used for the refractive index of BC can be, in principle, overcame by developing theoretical methods that go down to the most precise scale as possible, i.e., methods that are based on an atomistic description of the carbonaceous nanoparticles under consideration.

We have thus developed in Besançon a numerical method called the Dynamic Atomic Dipole Interaction (DADI) model, which is devoted to compute optical properties of carbonaceous nanoparticles, provided that the positions and the frequency-dependent polarizabilities of each type of atoms constituting the particles are defined [33, 34, 35, 36, 37]. Whereas realistic atomic positions in model nanoparticles can be obtained by, e.g., performing molecular dynamics simulations guided by experimental results (such as those coming from high-resolution electron microscopy studies [15, 38, 39, 40]), obtaining accurate values for polarizabilities appears as a trickier task, although it has been shown that reasonable MAC values for BC nanoparticle models can be computed when using frequency-dependent atomic polarizabilities extracted from available experimental data obtained on graphite [33, 34, 35].

In real environment, BC is usually made of aggregates of more or less spherical primary nanoparticles, presenting different fractal structures and compacities [12, 14]. Thus, it is expected that optical properties of BC would depend on the morphology of these aggregates, on their coating, on the degree of mixing with the coating, and on the refractive index of the corresponding materials [41, 42, 43, 44]. For instance, it has been shown that overlapping and necking between primary nanoparticles forming BC aggregates could have a strong influence on the depolarization of soot aggregates and should be considered in order to achieve good agreement between the calculated depolarization and the experimentally determined one [45]. However, taking into account, as precisely as possible, all these ingredients in theoretical approaches with the goal of interpreting experimental measurements and/or observations still remains challenging [46, 47, 48].

Here, we thus made use of our DADI model to compute optical properties, in the UV-Visible range, of two carbonaceous primary nanoparticles described at the atomic scale, with a special focus on three situations commonly arising in soot, namely separate, touching, and interpenetrating primary nanoparticles. Molecular dynamics simulations based on a reactive interatomic interaction potential have been performed to get the atomic coordinates of the carbons in the three configurations considered, and the graphite parametrization has been used for defining the polarizability tensors of the carbon atoms. More precisely, carbon atoms

have been assigned either anisotropic or isotropic polarizability tensors depending on their environment, as in our previous works [33, 35]. This allowed us to characterize the influence not only of the different relaxations of the atomic positions in these three situations, but also of the change of the resulting atomic polarizabilities, especially in the touching and coalescence zones. As stated above, the atomistic approach on which the DADI model is based avoids the thorny question of defining a priori a refractive index for the BC primary particles, more particularly in the coalescence zone, which would otherwise be a prerequisite for using other theoretical methods such as DDA [13]. On the contrary, we even propose here a theoretical method to compute this refractive index based on results obtained with the DADI model combined to the standard equations of the Rayleigh Debye-Gans approximation.

In Section 2, we briefly recall the details of the methodology used to model the primary nanoparticles and their interpenetration, together with the main ingredients of the DADI method and of the calculations of the refractive indices for BC nanoparticles. The results of the MAC for the systems considered are given in Section 3 and those for the refractive indices in Section 4. The main conclusions of this study are summarized in Section 5.

2. Computational details

2.1. The DADI model

Although the parametrized semi-empirical DADI model has been extensively presented in previous papers [33, 34, 35, 37], a brief overview is given here to recall the main ingredients of this numerical approach which allows computing the optical properties of large carbonaceous systems, on the basis of their atomistic details.

Indeed, following the classical equations of the DDA method [31, 32] with the Cartesian coordinates, and using the frequency-dependent atomic polarizability tensor of each atom as in the point dipole interaction (PDI) approach [49, 50, 51], the dipole induced on the atom i, by an external electric field $\vec{E}_0(\vec{r}_i, \omega)$ at the position \vec{r}_i of this atom, as well as by the induced dipoles of all the surrounding atoms, can be self-consistently calculated at the circular frequency ω , as

$$\vec{\mu}_i(\omega) = \bar{\bar{\alpha}}_i(\omega)\vec{E}_0(\vec{r}_i,\omega) + \sum_{j=1}^N \bar{\bar{\alpha}}_i(\omega)\bar{\bar{T}}(\vec{r}_i,\vec{r}_j,\omega)\vec{\mu}_j(\omega)$$
(1)

where $\bar{\alpha}_i(\omega)$ is the frequency-dependent atomic polarizability tensor of the atom i, and \bar{T} is the interaction tensor that can be computed from the double gradient of the vacuum Green's generalized function for the Helmholtz equation, as

$$\bar{\bar{T}}(\vec{r}_i, \vec{r}_{j \neq i}, \omega) = -\frac{1}{\epsilon_0} (\nabla_{\vec{r}_i} \otimes \nabla_{\vec{r}_j} + \frac{\omega^2}{c^2} \bar{\bar{I}}) (-\frac{e^{i\frac{\omega}{c}|\vec{r}_i - \vec{r}_j|}}{4\pi |\vec{r}_i - \vec{r}_j|})$$
(2)

where c is the speed of light, ϵ_0 the vacuum permittivity and \bar{I} the identity tensor.

Because in the DADI model the point dipoles are in fact atoms, they are much smaller than the discretization volumes usually defined in the DDA approach [31, 32]. Hence, the i = j terms of the interaction tensor \bar{T} are assumed to simplify as

$$\bar{\bar{T}}(\vec{r}_i, \vec{r}_i, \omega) = i \frac{2}{3} \frac{\omega^3}{c^3} \frac{1}{4\pi\epsilon_0} \bar{\bar{I}}.$$
 (3)

Eq. 1 is thus a $3N \times 3N$ matrix system whose resolution gives a $3 \times 3N$ vector containing the dipoles $\vec{\mu}_i(\omega)$ on each atom, corresponding to three values of \vec{E}_0 successively applied along the three (Cartesian) coordinate axes (as in PDI). Once all the dipoles have been self-consistently computed, they can be used to calculate global particle polarizabilities and optical quantities such as scattering, extinction and mass absorption cross sections. Note that the extinction and scattering cross sections can also be used to estimate the refractive indices of the system under consideration, as explained further.

2.2. Soot primary nanoparticle models

To calculate the optical properties of BC nanoparticles on the basis of their atomistic characteristics, the first ingredient of the DADI method is the Cartesian coordinates of each atom in the system under consideration [35, 37].

To get such information, we have taken into account that BC particles have been reported to result from aggregation of more or less spherical primary nanoparticles [14, 23, 52, 53], these primary nanoparticles being reasonably modeled, at the atomistic level, by carbon buckyonions, i.e., spherules made of carbon layers arranged in a concentric way and containing a certain amount of defects such as missing atoms [35, 54, 55]. Note that the term spherule will be used below instead of carbonaceous spherule, for simplicity, and in our approach, a spherule will therefore define our model of primary soot nanoparticle.

Here, a single spherule has been modeled by the three-shell fullerene $C_{540}@C_{960}@C_{1500}$ from which a certain amount of C atoms have been randomly removed on each shell to create holes, modeling nanopores (i.e., defects) within the bulk and at the surface of the spherule. On the two innercore fullerenes, 7 % of C atoms have been randomly removed whereas 10 % have been taken out on the surface shell (i.e., the largest C_{1500} fullerene), because experiments have clearly revealed that the outer shell of the soot primary nanoparticles is more defective than the inner ones [15]. Note that the separation between two successive shells is equal to 3.4 Å, in accordance with the experimental observations [15]. Overall, 247 C atoms have thus been removed, leading to a defective spherule that contains 2753 C atoms and presenting the main ingredients characterizing rather mature soot.[15]. This spherule has an external diameter of 36.4 Å, which is at the lower limit of the observed size distribution for soot primary particles, especially those produced by aircraft.[56, 57] Larger spherules can of course be considered, however, at the expense of the corresponding calculation cost.

Then, to investigate the effect of the coalescence on the optical properties of BC nanoparticles, three situations have been especially considered, in which two identical spherules have been considered as being either well-separated, or in close contact with each other, or interpenetrated.

To model these situations, the single spherule has simply been duplicated to create (thanks to a short home-made Python script) a system that consists of two separated, identical spherules, such that the distance between their centers of mass d is initially set to 39.4 Å. Then, this distance has been decreased such that the spherules come just in contact (d = 36.4Å) or are interpenetrated (d = 31.4 Å). Because these situations (especially the two latter ones) do not correspond to any equilibrated state, each of these three situations has been used as the starting point for molecular dynamic (MD) simulation runs, aiming at obtaining the Cartesian coordinates of the corresponding 5506 atoms in a relaxed system. These MD runs have been performed using the open-source code LAMMPS [58] and according to the following relaxation procedure: first, an energy minimization has been performed by using the conjugate gradient method, that has then been followed by a short MD run performed at 5 K, on the N,V,T ensemble. For the MD runs, a timestep of 1 fs has been used and a total of 100,000 timesteps has been considered, i.e., the total duration of the simulation has been set to 0.1 ns. The interactions between C atoms have been described by using the Adaptative Intermolecular Reactive Empirical Bond Order (AIREBO) potential model [59]. Of course, such a quick relaxation procedure cannot lead to a perfectly optimized structure of minimum energy (which would be a quite trickier task due to the large number of atoms involved). Nevertheless, it leads to configurations that are sufficiently different from the initial ones to expect impact on the DADI results (as it will indeed be shown below). In addition, the relaxation is able to give structures in which acceptable configurations for the C atoms have been reached, especially in the contact and coalescence zones. This has been checked by calculating radial distribution functions (not shown) of the C-C distances which showed that nearest-neighbor C atoms are indeed located at distances less than 0.16 nm from their next neighbors (as indicated by the first peak of the distribution), which may thus corresponds to the formation of chemical C—C bonds.

The relaxed systems considered in the DADI calculations thus present the main geometric characteristics of BC nanoparticles in three typical situations, in which these nanoparticles are either located far apart (relaxed separated system), or just colliding (relaxed touching system), or already coalescing (relaxed interpenetrated system). The corresponding structures are shown in Figure 1 as an illustration.

2.3. Carbon atomic polarizabilities

The spherules considered here only contain carbon atoms. The choice of a parametrization for carbon atomic polarizabilities in such structures remains arbitrary, since, to date, no experiments have been carried out to discriminate between different sets of parametrization. However, using graphite data appears reasonable to get qualitative results [35], as soot pri-

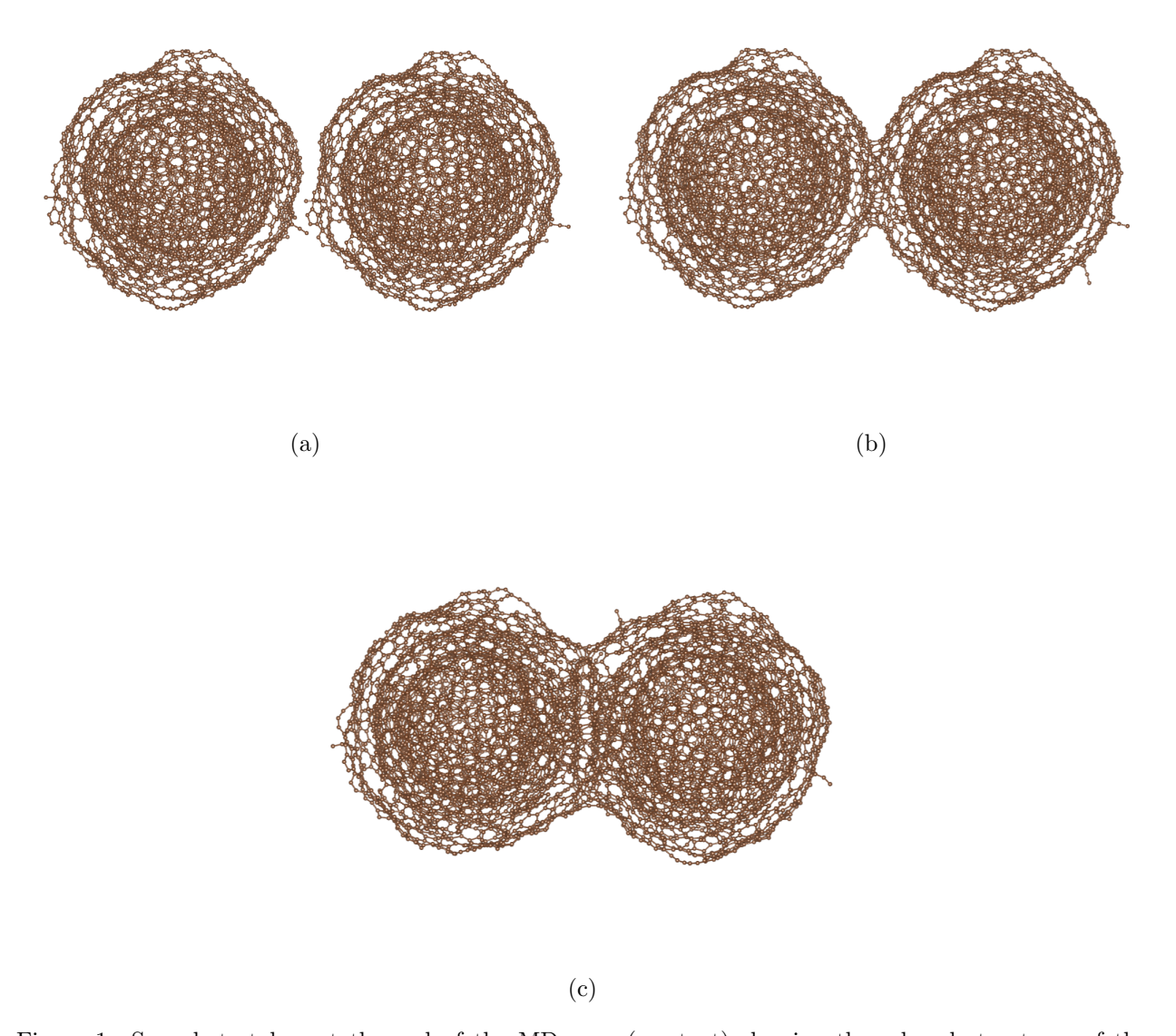


Figure 1: Snapshots taken at the end of the MD runs (see text) showing the relaxed structures of the spherules considered in the DADI calculations. Three typical situations have been modeled, namely (a) separated, (b) in contact, and (c) interpenetrated spherules. Carbon atoms are represented as small spheres and covalent bonds are materialized by connections.

mary nanoparticles are actually made of graphite-like nanoclusters [15]. Thus, polarizability values calculated from the permittivity values given by Draine for graphite [60] (which will be thus called "Draine parametrization") have been chosen here, in coherence with our previous works [33, 34, 35]. These permittivity values have been converted to polarizability values using the generalized Clausius-Mossotti relation as:

$$\frac{N}{V} \frac{\alpha_a^{local}(\omega)}{\epsilon_0} = \frac{\epsilon_a(\omega) - 1}{1 + B_a(\epsilon_a(\omega) - 1)} \tag{4}$$

where the index a labels one of the three principal directions defining the local basis frame and N/V is the atomic density. The coefficients B_a are the depolarization factors given by Senet et al. [61] and confirmed by Andersen and Bonderup [62] for graphite, i.e., $B_{\perp} = -0.606$ and $B_{//} = 0.803$.

Note that, following our previous works [33, 34, 35], the local basis frame has been defined, for any C atom surrounded by three neighbors, by two unit vectors parallel to the plane defined by these three nearest neighbors and one unit vector perpendicular to this plane. In this frame, C atoms with three neighbors are thus characterized by an anisotropic polarizability tensor with two parallel identical and one (different) perpendicular components, as any sp^2 hybridized C atom in graphite [60]. Thereafter, these atoms will be named C3 carbons, for convenience. However, by construction our spherules also contain point defects that correspond in fact to C atoms having less or more than three neighbors. Because these atoms (hereafter named C1, C2, and C4, depending on their number, 1, 2, and 4, of neighbors) are expected to have different polarizabilities from that of C3, they have been (arbitrarily) characterized by an isotropic polarizability tensor, i.e., a diagonal tensor in which all three diagonal elements have the same value, obtained by calculating the arithmetic average of the (two) parallel and the perpendicular components of the polarizability tensor of graphite [35].

Proceeding this way, computations with the DADI model have been run using different atomic polarizability tensors for C1, C2, or C4 (isotropic) on the one hand and C3 (anisotropic) carbon atoms, on the other hand, depending on their local environment in the spherules. Note that the respective number of these C atoms is strongly influenced by the interpenetration process of the two spherules, as resulting from the MD simulations (see below). In our approach, the coalescence thus impacts not only on the positions, but also on the polarizability values of the carbon atoms.

2.4. Computation of complex refractive indices

A commonly used method for the evaluation of the radiative properties of nanometer-scale particles relies on the Rayleigh–Debye–Gans approximation (RDG). This approach presents the advantage of simplicity and adaptations have been proposed for fractal aggregates as those formed by soot primary nanoparticles [25, 63, 64, 65, 66, 67].

Thus, following RDG equations, the scattering and absorption functions, namely F(m) and E(m), can be computed, at a given wavelength, from the scattering and extinction cross sections (C_{sca} and C_{ext} , respectively), as follows:

$$F(m) = \frac{\lambda^4 C_{sca}}{24\pi^3 V^2} \tag{5}$$

and

$$E(m) = \frac{\lambda C_{ext}}{6\pi V} \tag{6}$$

where λ is the wavelength in nm at which the refractive (complex) index m is computed, and V is the common average volume of the whole carbonaceous system computed as N times the volume of a carbon atom (this value is calculated using the density value of 1.8 g.cm⁻³ which is commonly used for BC [24]).

The originality of our approach is that C_{sca} and C_{ext} have been calculated with the DADI model for the spherules considered here. Then, knowing F(m) and E(m) from these DADI calculations and using their expressions as a function of the complex refractive index m given by:

$$F(m) = \left| \frac{m^2 - 1}{m^2 + 2} \right|^2 \tag{7}$$

and

$$E(m) = \operatorname{Im}\left(\frac{m^2 - 1}{m^2 + 2}\right),\tag{8}$$

it is straightforward to compute the square of the complex refractive index m^2 as

$$m^2 = \frac{1+2z}{1-z} \tag{9}$$

where z is given by

$$z = \pm \sqrt{F(m) - E(m)^2} + iE(m). \tag{10}$$

Because in a Fortran code, the square root of a complex number returns the principal value of the square root, the computed z has a non-negative real part (checks were performed in the code to ensure the consistency of this solution). By writing now the complex refractive index as $m = n + i\kappa$, we have $m^2 = (n^2 - \kappa^2) + 2in\kappa$. Because of the following equation:

$$E(m) = \operatorname{Im}\left(\frac{m^2 - 1}{m^2 + 2}\right) = \frac{3\operatorname{Im}(m^2)}{(\operatorname{Re}(m^2) + 2)^2 + (\operatorname{Im}(m^2))^2},\tag{11}$$

Table 1: Number n_{Ci} of atoms of the various types (i=1,2,3, and 4, depending on the number of nearest neighbors) for the three systems considered in the DADI calculations (each system contains a total of 5506 carbon atoms). Because only C3 atoms are characterized by an anisotropic polarizability tensor (see text), $n_{C_{aniso}} = n_{C3}$, whereas $n_{Ciso} = n_{C1} + n_{C2} + n_{C4}$. Note that the number of C4 atoms, corresponding to sp³-like hybridization (i.e., 4 nearest neighbors), has also been indicated.

Configurations	$n_{C_{aniso}}$	$n_{C_{iso}}$	n_{C4}	$r = \frac{n_{C_{aniso}}}{n_{C_{iso}}}$
Separated spherules	4554	952	0	4.78
spherules in contact	4532	974	33	4.65
Interpenetrated spherules	4596	910	74	5.05

 $\operatorname{Im}(m^2)$ is of the same sign as E(m). Because E(m) is always positive, n and κ must be of the same sign. With the chosen $e^{-i\omega t}$ convention, κ has to be always positive for a passive (absorbing) medium. Therefore, n is also positive, and it finally comes:

$$n = \sqrt{\frac{|m^2| + \text{Im}(m^2)}{2}},\tag{12}$$

and

$$\kappa = \sqrt{\frac{|m^2| - \operatorname{Im}(m^2)}{2}}. (13)$$

This approach, which combines the classical equations of the RDG method and the calculations of the cross sections with the DADI model, has the distinctive advantage of being able to compute the global refractive index, as a function of wavelength, of large carbonaceous structures made of thousands of atoms, directly from their atomistic details, i.e., the knowledge of the frequency-dependent polarizabilities and of the Cartesian coordinates of the atoms forming the systems under investigation. In particular, any assumption on the shape of the carbonaceous structure is thus avoided and the method allows us to investigate the influence of any structural or chemical change, even small and/or localized, on the optical properties of the system.

3. Results

3.1. Mass absorption cross sections

Before the calculations with the DADI model are performed, the exact number of atoms of each atom type (carbon C1 to C4) has been computed, allowing to discriminate the carbon atoms characterized by an anisotropic polarizability tensor (C3 atoms) from those characterized by an isotropic polarizability tensor (C1, C2 and C4 atoms), as explained above (see Section 2.3). The corresponding values are given in Table 1.

Figure 2 shows the MAC calculated using the DADI model for the three situations considered here, i.e., two (identical) spherules which are well separated or in contact with

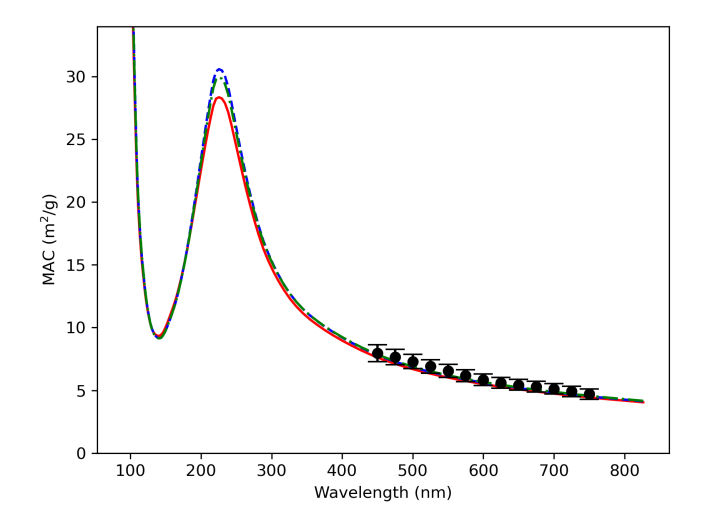


Figure 2: Mass absorption cross sections of two separated (dashed blue curve), in contact (dashed-dotted green curve), and interpenetrated (red curve) spherules, as calculated with the DADI model, between 100 and 800 nm. Experimental data coming from Ref. [68] have also been indicated as small black spheres.

each other or interpenetrated. Calculations have been performed between 100 and 800 nm, using the parametrization for the atomic polarizabilities which is based on the graphite data [60].

As shown in Figure 2, the MAC curves are characterized by a large absorption peak in the near UV, the position of which being slightly shifted by about 4 nm, and its maximum intensity decreasing by about 8 %, upon the interpenetration of the two spherules. It is interesting to note that this variation of the MAC intensity obtained directly from the atomistic details of the system and the DADI model is in line with the correction factor of about 1.1 (i.e., a modification of 10 %) which has to be applied to results obtained with the RDG-FA theory to take into account the overlapping effects of soot primary nanoparticles [42]. In addition, it is worth mentioning that the present MAC values are in very fair agreement with experimental measurements performed over a wavelength range of 450–750 nm for soot of a methane flame, as shown in Figure 2 (note that, as far as we know, this is a rare example of available experimental data in such an extended wavelength range) [68].

Looking especially at 550 nm (see the results given in Table 2), the MAC calculated for the two separated (identical) spherules, is equal to 6.16 m^2/g , a value which is a bit lower than the standard value of $7.5 \pm 1.2 \ m^2/g$ recommended by Bond and Bergstrom in 2006 [24]. However, the present value is coherent with other numerical/theoretical estimations of the MAC values of soot aggregates (see Table 4 of Ref.[13]). It is also worth noting that, at this wavelength, the MAC value does not significantly differ from one configuration to another one (decrease of about 2.6 % upon interpenetration), unlike in the near UV where a

Table 2: Mass Absorption Cross sections as calculated with the DADI model, at 250 and 550 nm, for the three configurations of the spherules considered here.

Configurations	Peak posi-	MAC	at	MAC	at
	tion (nm)	250	nm	550	nm
		(m^2/g)		(m^2/g)	
Separated spherules	223	25.80		6.16	
Spherules in contact	223	25.38		6.19	
Interpenetrated spherules	227	24.32		6.00	

decrease of about 5.7 % is calculated for the MAC values at, e.g., 250 nm (see Table 2). The present results thus give indications that experimental measurement of MAC values for BC should rather be performed in the near UV than at visible wavelengths, to observe intensity variations and peak position shifts related to morphological differences within the particles constituting BC.

Because, in the DADI model, frequency-dependent atomic polarizabilities are directly used to compute the MAC of carbonaceous nanoparticles, the choice of the corresponding parametrization remains a cornerstone of the model.

Thus, to ensure that the effects of interpenetration as evidenced here on the calculated MAC values do not depend on the parametrization that has been initially chosen (i.e., parametrization based on the graphite properties [60]), another set of polarizability values has also been used to compute the optical properties of the systems considered here. The corresponding calculations have been based on carbon atomic polarizabilities derived from the experimental permittivity values given by Sohmen et al. for the C_{60} molecule [69]. Note that, although the values coming from C_{60} are certainly better suited for highly curved carbonaceous structures, they have been chosen here because, as those coming from graphite parametrization, they are not influenced by the presence of any H atom, in contrast with polarizability values that have been recently computed for polycyclic aromatic hydrocarbon molecules [37].

The MAC values obtained at 250 nm with the C_{60} parametrization [69] decreases from 21.80 to 21.05 m^2/g (i.e., a decrease of about 3.5 %) upon the interpenetration of the two spherules, similarly to what has been calculated using the graphite parametrization [60]. By contrast, the MAC value at 550 nm increases from 6.78 (separated spherules) to 7.51 m^2/g (interpenetrating molecules) when using the parametrization coming from C_{60}

It is also worth noting that, in our soot modeling, we do not made any difference between the non-graphitized carbon atoms (named C1, C2 and C4) themselves which have been assigned the same isotropic polarizability tensor. However, this difference could be easily taken into account in the DADI model if the corresponding atomic polarizability tensors are known, which is, unfortunately, not the case yet for C1 and C2. Moreover, although atomic polarizability tensors are available for the C4 atoms [37], they have been fitted for

aliphatic carbons, i.e., by taking into account the presence of C-H bonds. Because the spherules modeled here do not contain any H atoms, using the polarizability values obtained for aliphatic carbons would be questionable. Thus, rather than characterizing the possible effects coming from various parametrizations of the non-graphitized carbons, a focus has been made on the influence of other parameters, using the available polarizability tensors for C atoms (i.e., those coming from graphite). Indeed, as highlighted above, the modifications of the MAC values upon the interpenetration of the two spherules mainly result from the local polarizability changes coming from the evolution of the number of neighbors of some carbon atoms upon the relaxation of the atomic positions. To better identify the underlying origin of these variations of the MAC values properties, a detailed analysis of the effect of each parameter modified during the interpenetration process has thus been performed. Indeed, contrarily to real situations in which the influence of all these parameters would be hardly distinguishable, the modeling approach allows to focus separately on i) the ratio between the number of anisotropic and that of isotropic C atoms $(r = C_{aniso}/C_{iso})$, ii) the distribution of the different carbon atom types (i.e. C1, C2, C3 and C4) in the particles, iii) the orientation of the anisotropic polarizability tensors, and iv) the positions of the carbon atoms, to determine which parameter has the largest influence, if any.

3.1.1. Effect of the ratio between the number of anisotropic and that of isotropic carbons

In our approach, the ratio $r = C_{aniso}/C_{iso}$ is directly linked to the number of nearest neighbors of each carbon atom in the system. Indeed, as explained above, the atomic polarizability tensor of C3 has been given the values of the anisotropic frequency-dependent polarizability tensor coming from graphite data whereas all the other carbons (C1, C2, and C4, i.e., carbons with one, two or four nearest neighbors) have been assigned an isotropic frequency-dependent polarizability tensor (obtained by averaging the diagonal components of the anisotropic polarizability tensor).

As reported in Table 1, the ratio r is modified by the interpenetration process because the number of nearest neighbors of some carbon atoms changes upon the relaxation of the interpenetrated spherules. Thus, to check the specific influence of r variations, the MAC of a model system in which the geometry has been fixed and only the ratio r has been modified, has been calculated as follows.

The configuration in which the spherules are interpenetrated has been chosen, as a reference for the fixed geometry. In this configuration, the actual ratio r is equal to 5.05 (see Table 1).

Then, keeping the same configuration, the ratio r has been decreased by randomly selecting carbon atoms (everywhere in the spherules) and arbitrarily switching their polarizability tensor from anisotropic to isotropic, until the ratio r reaches the value of 4.78. It has to be noted that the Cartesian coordinates of the selected atoms have not been modified, ensuring that only the ratio r has changed.

As shown in Figure 3, in the visible range of the spectra (350-750 nm), the MAC value

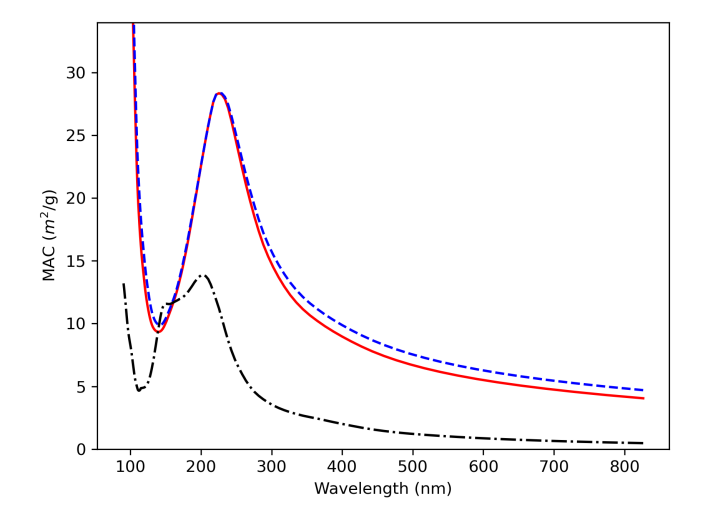


Figure 3: Mass absorption cross sections calculated with the DADI model for two coalesced spherules containing different numbers of anisotropic vs. isotropic carbon atoms (see text), corresponding to r = 5.05 (red curve), r = 4.78 (dashed blue curve), and r = 0 (dotted-dashed black curve).

increases by about 12 % while r decreases from 5.05 to 4.78, in accordance with the results shown in Table 2. However, in the UV range, the MAC curves are almost undistinguishable (especially in the region of the maximum), in contrast with the behavior exhibited on Figure 2 upon interpenetration of the two spherules.

Because the two r values considered above correspond to a polarizability change (from anisotropic to isotropic polarizability tensor) of a few tens of carbon atoms, only (see Table 1), the extreme situation in which all the atoms have been assigned an isotropic instead of an anisotropic polarizability tensor has also been considered in the DADI calculations. In this case, r = 0, and the corresponding MAC curve, also given in Figure 3 (dashed-dotted black curve), significantly differs from the two other ones (r = 5.05 and r = 4.78), confirming thus that considering isotropic polarizability tensors in our spherules instead of anisotropic ones does indeed change the corresponding MAC curves, as already observed in a previous work [35].

The demonstration is thus made here that MAC changes are, at least partly, driven by the polarizability changes during the coalescence of the spherules.

3.1.2. Effect of the distribution of the carbon atom types

To better assess the influence of the positions where the polarizability changes take place, we have again considered the configuration in which the two spherules are interpenetrated (r = 5.05), as a reference. However, the polarizability tensors have now been randomly distributed on the carbon atoms such that a C atom has been assigned an isotropic or an

anisotropic tensor, regardless of its number of neighbors, the constraint being only to keep the ratio r = 5.05 unchanged.

It should be mentioned that when doing this, it happened that 755 C atoms had to be assigned an anisotropic tensor although they do not have three next neighbors. But, as explained in Section 2.3, the parallel and perpendicular components of the anisotropic polarizability tensor have to be defined with respect to a local frame which is determined with respect to the plane defined by the location of the three next neighbors. Thus, to overcome this situation and to be able to perform the DADI computations with the anisotropic polarizability tensors, it has been arbitrarily decided to choose, for these C atoms, the axes of the global frame as principal axes of the polarizability tensor, even though we are aware that this situation is a purely virtual case. Nevertheless, it allows the desired comparison in the framework of our theoretical approach. Furthermore, to better estimate the influence of this assumption, two calculations have been performed, one in which the perpendicular components of the anisotropic polarizability tensors are all defined along the z-axis of the global frame and the other one in which it is along the y-axis of the global frame.

The corresponding MAC values, between 100 and 800 nm, are given in Figure 4. In this Figure, the MAC curve calculated for the reference system with the real distribution of polarizability tensors (already shown in Figure 2) has also been reported for comparison (note that real distribution means that each carbon atom has been assigned the anisotropic or the isotropic polarizability tensor which depends on its actual neighborhood).

First of all, the results given in Figure 4 show that the arbitrary orientation of the 755 anisotropic tensors randomly distributed in the system has very little influence on the corresponding MAC curves which are almost superimposed. By contrast, MAC values appear influenced by the location of the anisotropic tensors. Indeed, the main peak in the UV region of the spectra is blue shifted by more than 10 nm when considering random distribution of the tensors rather than their real positions, while the MAC value at the maximum of this peak decreases by about 13 %. In addition, above 300 nm, the MAC values calculated when considering the real distribution of polarizability tensors are about 10-12 % smaller than those calculated with the random distribution of these tensors.

These results emphasize the role played on the optical properties by the exact location where the change of the polarizability tensors (anisotropic vs. isotropic) takes place when geometric restructuring of carbonaceous particles arises upon their interpenetration.

3.1.3. Effect of the orientation of the anisotropic polarizability tensors

Here, we focus on the role that the orientation of the anisotropic polarizability tensors may play on the optical properties of the system, in the DADI calculations. We again consider as reference the situation in which the two spherules are interpenetrated, with the ratio r = 5.05 (i.e. the real ratio), and the atomic polarizability tensors are at their correct location (i.e., C3 atoms have been assigned anisotropic polarizability tensors while the other atoms have been assigned isotropic ones). Thus, the calculated MAC curve is that already

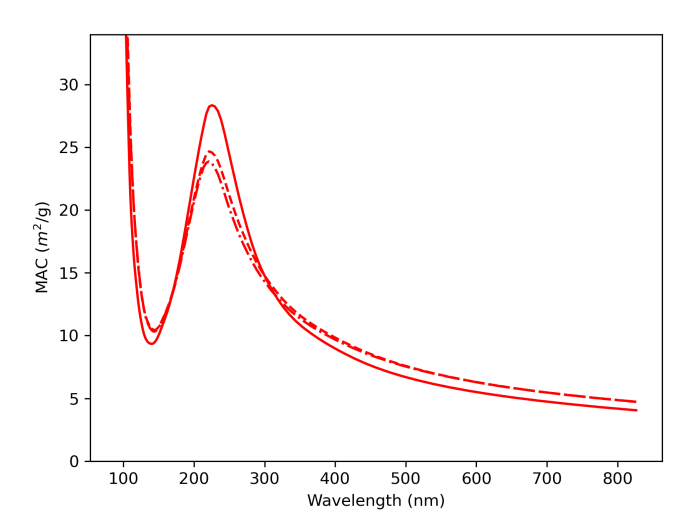


Figure 4: Mass absorption cross sections calculated with the DADI model for two interpenetrated spherules containing the same number of anisotropic vs. isotropic carbon atoms, corresponding to r=5.1, but differing by the location of the anisotropic polarizability tensors. The full red curve corresponds to the real distribution of the polarizability tensors, whereas the dashed and dashed-dotted red curves correspond to a random distribution of the atomic polarizability tensor, for which the perpendicular component of all the anisotropic polarizability tensors has been defined with respect to either the z-axis or the y-axis of the global frame, respectively.

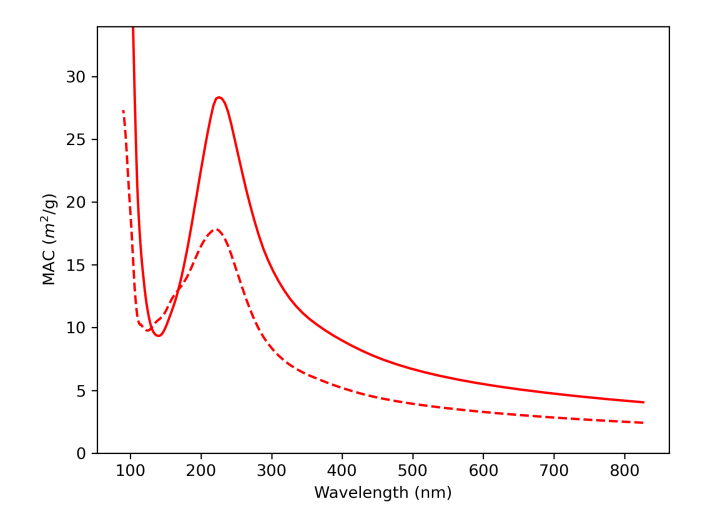


Figure 5: Mass absorption cross sections calculated with the DADI model for two coalesced spherules with r = 5.1 with the consideration (red curve) or not (dot-dashed red curve) of the correct orientation of the anisotropic tensors.

given in Figure 2. But we have also performed the DADI calculations by considering that all the anisotropic polarizability tensors are defined in the same global frame, rather than in their respective local frame as in Figure 2. As an illustration, we have chosen to define the perpendicular components of these tensors along the z-axis of the global frame. Note that doing this means that using rotation matrices in Eq. 1 is no more necessary because the axes of the global frame are aligned with the three directions successively chosen for the incident electric field (see paragraph 2.1). As already mentioned above, this situation corresponds to a purely theoretical case, for analysis purpose.

The MAC curves calculated in the real situation and in the case for which all the anisotropic polarizability tensors are defined in the same frame are compared in Figure 5, in which it is clearly evidenced that the MAC curve is significantly blue shifted in this latter case with respect to the former one, and that the corresponding MAC values are largely smaller. These results illustrate the importance of defining the components of the anisotropic polarizability tensors with respect to their local frames (i.e., those attached to the C atoms which have been assigned the anisotropic tensors) instead of with respect to the same global frame.

Finally, an additional test has been performed by comparing the MAC curves obtained when considering the real and the random distributions of the anisotropic polarizability tensors (still with the constraint r = 5.05), and when defining the components of all these tensors in the same global frame. In the corresponding calculations, the perpendicular component of the anisotropic tensors has been defined with respect to the z-axis of the

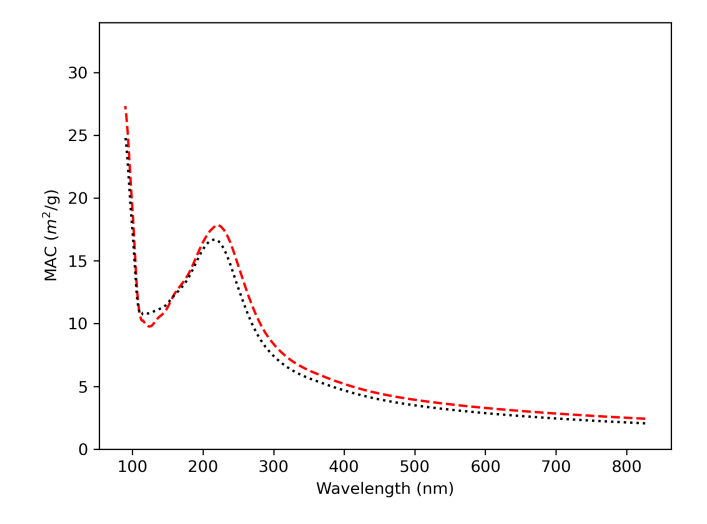


Figure 6: Mass absorption cross sections calculated with the DADI model for two separated spherules containing the same number of anisotropic vs. isotropic carbon atoms (see text), corresponding to r=5.1, but differing by the locations of the C atoms on which anisotropic polarizability tensors are assigned. Calculations have been performed when considering a random (dotted black curve) or the real (dashed red curve) distribution of these carbon atoms. In both cases, the perpendicular component of every anisotropic tensor is oriented along the z-axis, i.e., in the global frame rather than in the corresponding local frame.

global frame, as an example. Again, these calculations correspond to virtual situations, but they give the unique opportunity to focus on a system where only the locations of the anisotropic tensors have been modified, and not their orientation. The corresponding results are given on Figure 6 in which it can be seen that randomly distributing the anisotropic polarizability tensors clearly results in a blue shift of the MAC curve with respect to the situation where these tensors are located at their real position, as well as in smaller MAC values in the UV-Visible range. Thus, by freeing oneself from the exact orientations of the tensor components, these additional calculations highlight the role played by the positions of the C atoms to which anisotropic polarizability tensors are assigned.

3.1.4. Effect of the carbon atoms location

In this last series of calculations, the tensor orientations have been totally disregarded by considering that all C atoms have been assigned an isotropic polarizability tensor (coming from the graphite parametrization, as explained before). This means, by definition, that any polarizability change will be disregarded in the DADI calculations upon restructuration of the spherules (because the constraint r = 0 has been imposed).

The MAC curves have then been computed for two separated and two interpenetrated spherules, by taking into account the real positions of their atoms. The corresponding results, obtained between 100 and 800 nm with the DADI model, are given in Figure 7.

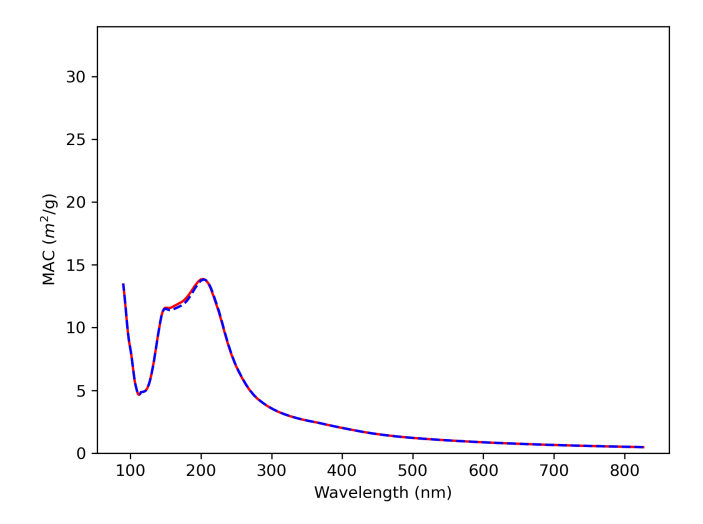


Figure 7: Mass absorption cross sections calculated with the DADI model for two well separated (dashed blue curve) or interpenetrated (red curve) spherules, in which only atomic isotropic polarizability tensors have been considered.

As it can be seen, the two MAC curves are almost superimposed on the entire range of wavelengths, which is coherent with the fact that the spherules are of size much smaller than the wavelength, a situation that corresponds to the Rayleigh approximation. It can be thus concluded that, for these small spherules, the geometrical changes (i.e., modifications in the atomic positions) inherent in interpenetration cannot, by themselves, result in a modification of their optical response (MAC curves), if the corresponding atomic polarizabilities remain unchanged.

4. Calculations of the refractive indices

The refractive indices for the systems considered here have been calculated, as a function of the wavelength between 100 and 800 nm, in the three situations described above, i.e., when the two spherules are separated, just in contact or interpenetrated, by using the model developed in Section 2.4.

The real (n) and imaginary (κ) parts of the calculated refractive indices are shown in Figure 8 for the three situations considered here, as a function of the wavelength. In addition, their corresponding values at 550 nm, a wavelength typically used as a reference in the literature [13, 70], have been given in Table 3.

First of all, it is worth noting that the results obtained here on the basis of a combination between RDG and DADI models are perfectly compatible with those recently reported for BC particles at 550 nm [13]. Indeed, it has been shown that, to explain measured optical

Table 3: Values of the real (n) and imaginary (κ) parts of the refractive index calculated at the wavelength of 550 nm for the three situations of the two spherules considered here. The corresponding ratio $r = C_{aniso}/C_{iso}$ is also recalled, for information.

Configurations	$r = \frac{n_{C_{aniso}}}{n_{C_{iso}}}$	n (550 nm)	$\kappa (550 \text{ nm})$
Separated spherules	4.78	1.74	0.90
Spherules in contact	4.65	1.71	0.90
Interpenetrated spherules	5.05	1.65	0.87

properties of soot, the most plausible values of n and κ are expected to be in the ranges 1.5 < n < 1.86 and $0.68 < \kappa < 1$ [13]. In addition, these values of n and κ should be constrained by 0.32 < E(m) < 0.4 [13], a condition which is again verified in our approach which gives, from Eq. 8, a value of E(m) = 0.34, at 550 nm.

As it can be seen in Figure 8, the real and imaginary parts of the refractive indices are both impacted by the configurations of the two spherules, especially above $\lambda=250$ nm, with almost constant differences of about 6 % for $n(\lambda)$ and 4 % for $\kappa(\lambda)$ between the situation where these spherules are well-separated and that of interpenetrated spherules. Note, however, that only the values of n appear to be perceptibly modified when the system changes from separated spherules to spherules in contact. Clearly, the strongest modification of the refractive index values is calculated when the two particles are interpenetrated, a situation which can be related to the fact that the relaxation upon interpenetration leads to a polarizability change for about 1 % of the C atoms (as shown in Table 1), and to the increase from 4.78 to 5.05 of the ratio between the number of anisotropic and that of isotropic C atoms. Such small variations have already been shown to impact on the optical properties of carbonaceous (primary) nanoparticles when using the DADI model [35], and it is thus not surprising that similar effect is also seen on the refractive index values calculated here.

It is worth noting that the refractive index calculated with this C_{60} parametrization (see above) [69] is equal to 1.71 + i1.07 at 550 nm, the values of the real and imaginary parts of this index being both higher than those calculated with the graphite parametrization, but still remaining almost in the range of acceptable values for soot [13].

The refractive indices obtained above with the graphite parametrizations have then been used to calculate the optical properties of the spherules considered here in the framework of the T-matrix method, adapted for multiple spheres (MSTM code) [71, 72]. The mass absorption cross sections calculated with this T-matrix approach are given in Figure 9 and compared with the values directly obtained with the DADI model, for systems consisting of two well separated and two interpenetrated spherules. As it can be seen, a very good agreement is obtained between the two methods, in both situations. Indeed, in average, differences of about 7 and 8 % have been calculated between T-matrix and DADI results, for separated and interpenetrated spherules, respectively.

In addition, as shown on Figure 10, the interpenetration of the two spherules is responsible

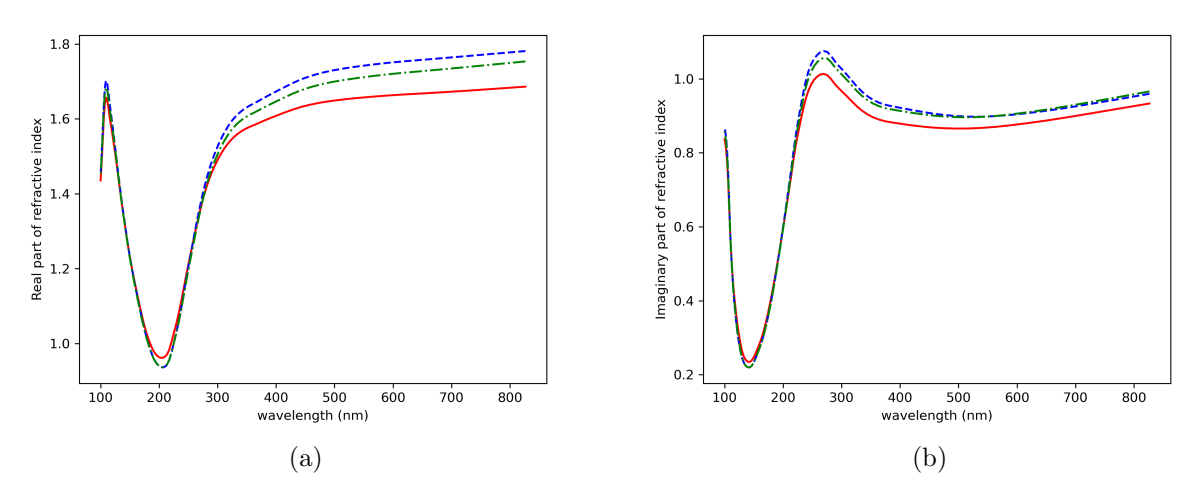


Figure 8: (a) Real and (b) imaginary part of the refractive index calculated for two identical soot spherules, between 100 and 800 nm, when considering three typical situations: separated (dashed blue curve), in contact (dashed dotted green curve) and interpenetrated (red curve) spherules.

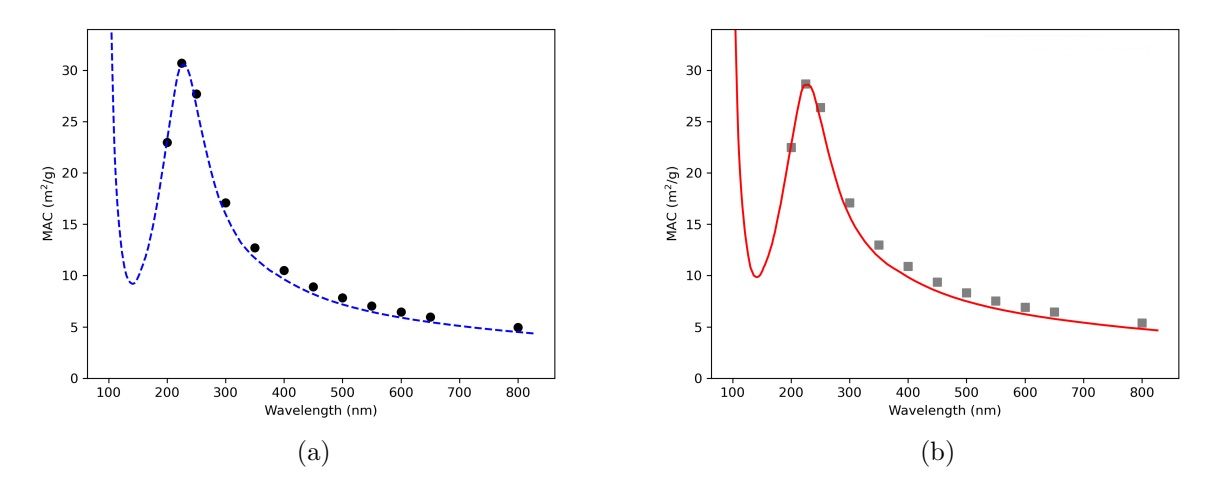


Figure 9: Comparison between the mass absorption cross sections calculated with the T-matrix (symbols) and the DADI approaches (doted lines) for the two separated (left) and the two interpenetrated (right) spherules.

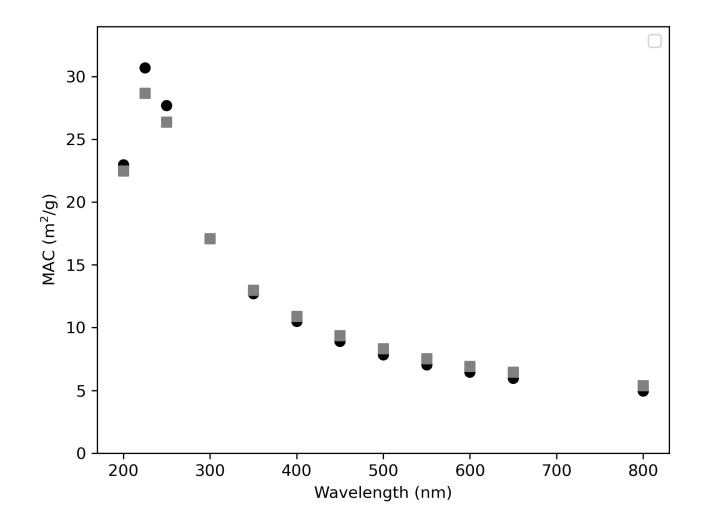


Figure 10: Mass absorption cross sections calculated with the T-matrix approach for two well separated (circles) and two interpenetrated (squares) spherules, in which refractive indices calculated with the DADI model have been considered.

for a small decrease of the MAC values calculated with the T-matrix method, confirming thus the results obtained with the DADI model. For instance, at 250 nm, this decrease upon interpenetration of the two spherules is equal to 5.7 % when calculated with the DADI model (see Table 2) whereas it is equal to 4.7 % when calculated with the T-matrix method.

Interestingly, this fair agreement between the T-matrix and the DADI results indicates that the refractive indices obtained here by taking into account the atomistic details of the spherules can be safely used as inputs in other theoretical, macroscopic approaches.

However, it should be kept in mind that because variations of the values of these refractives indices upon interpenetration of the spherules are related not only to localized polarizability changes in these spherules, but also directly to their structural relaxation, i.e., to the variation of the atomic positions in the spherules (as evidenced here), a correct estimation of these indices cannot be obtained without using a theoretical method based on the atomic description of the system, such as the DADI model.

5. Conclusion

Here, the DADI model has been used to investigate the influence of the coalescence of two carbonaceous nanoparticles on their optical properties. The results of the calculations have shown that the interpenetration of these spherules actually modifies the values of their refractive index and of their MAC by a few percent, and that the corresponding variations are tightly bound to local modifications of the system, with a subtle interplay between changes in both the atomic polarizabilities and the atomic positions. In other words, the restructuring of the close neighborhood of the carbon atoms upon coalescence is the key point to better assess the impact of soot ageing on their optical properties and, consequently, on their radiative forcing (climate impact). Thus, the less the soot primary particles are graphitized, the more they would contains isotropic C atoms, leading then to lower MAC values, as shown here.

From the theoretical point of view, atomistic modeling based on, e.g., the DADI method, would certainly be a reasonable way to obtain the requested precision, provided that accurate atomic polarizabilities are available. Meanwhile, sophisticated molecular dynamics simulations can certainly be considered to improve the modeling of the soot restructuring upon coalescence. The question remains on whether this level of precision can be attainable or not by local experimental probes such as high-resolution electronic microscopy (HRTEM).

In addition, changes in the optical properties of soot clearly appear to not only result from atomic displacements, but also from local changes in atomic polarizabilities. Formally, this therefore prevents using the same optical index to globally describe by macroscopic approaches any kind of soot, even with the same composition. On the contrary, different values of the refractive index may even appear necessary to take into account at least the particularity of the coalescence zone on the one hand, and the rest of the system on the other. Calculations at the atomic scale, e.g., via the DADI method, make it possible to overcome these constraints and allow the computation of refractive indices which are usable as inputs in macroscopic models, such as T-matrix, as shown here.

In further studies, considering the presence of other types of atoms as, e.g., oxygen or sulfur atoms, in the soot particles, as well as possible organic coating would be also required to better quantify the impact of soot ageing processes on climate forcing. Adding new types of atoms (in the structure or in the coating of the soot) in the DADI calculations is certainly feasible, provided that the corresponding frequency-dependent atomic polarizabilities are known, which could come from our inverse DADI method [37] fed by high-level quantum computation results (e.g., TD-DFT) or experimental results ideally performed in the near UV, for different soot particle compositions and morphologies.

Acknowledgements

This work has been supported by the EIPHI Graduate School (contract ANR-17-EURE-0002) and the Région Bourgogne-Franche-Comté. Computations have been performed on local facilities at Institut FEMTO-ST and on the regional supercomputer facilities of the Mésocentre de calcul de Franche-Comté. Prof. Zhao Wang, from the Department of Physics, Guangxi University (Nanning, China) is gratefully acknowledged for very useful comments and suggestions.

References

- [1] N. Islam, B. K. Saikia, An overview on atmospheric carbonaceous particulate matter into carbon nanomaterials: A new approach for air pollution mitigation, Chemosphere 303 (2022) 135027. doi:https://doi.org/10.1016/j.chemosphere.2022.135027.
- [2] M. A. Correa-Ochoa, R. Bedoya, L. M. Gómez, D. Aguiar, C. A. Palacio-Tobón, H. A. Colorado, A review on the characterization and measurement of the carbonaceous fraction of particulate matter, Sustainability 15 (11) (2023) 8717. doi:https://doi.org/10.3390/su15118717.
- [3] D. Contini, R. Vecchi, M. Viana, Carbonaceous aerosols in the atmosphere, Atmosphere 9 (5) (2018) 181:1–8. doi:https://doi.org/10.3390/atmos9050181.
- [4] M. O. Andreae, A. Gelencsér, Black carbon or brown carbon? The nature of light-absorbing carbonaceous aerosols, Atm Chem Phys 6 (10) (2006) 3131–48. doi:https://doi.org/10.5194/acp-6-3131-2006.
- [5] A. Laskin, J. Laskin, S. A. Nizkorodov, Chemistry of atmospheric brown carbon, Chem Rev 115 (10) (2015) 4335–82. doi:https://pubs.acs.org/doi/10.1021/cr5006167.
- [6] R. Wang, Y. Balkanski, O. Boucher, P. Ciais, G. L. Schuster, F. Chevallier, B. H. Samset, J. Liu, S. Piao, M. Valari, et al., Estimation of global black carbon direct radiative forcing and its uncertainty constrained by observations, J Geophys Res: Atmos 121 (10) (2016) 5948–71. doi:https://doi.org/10.1002/2015JD024326.
- [7] S. Sonwani, A. Yadav, P. Saxena, Atmospheric brown carbon: A global emerging concern for climate and environmental health, Management of contaminants of emerging concern (CEC) in environment 1 (2021) 225–47. doi:http://dx.doi.org/10.1016/B978-0-12-822263-8.00008-7.
- [8] D. Koch, A. Del Genio, Black carbon semi-direct effects on cloud cover: Review and synthesis, Atm Chem Phys 10 (16) (2010) 7685–96. doi:https://doi.org/10.5194/acp-10-7685-2010.
- [9] U. Lohmann, F. Friebel, Z. A. Kanji, F. Mahrt, A. A. Mensah, D. Neubauer, Future warming exacerbated by aged-soot effect on cloud formation, Nat Geosci 13 (10) (2020) 674–80. doi:https://doi.org/10.1038/s41561-020-0631-0.
- [10] P. Jaramillo, S. Kahn Ribeiro, P. Newman, S. Dhar, O. Diemuodeke, T. Kajino, D. Lee, S. Nugroho, X. Ou, A. Hammer Strømman, J. Whitehead, Transport, in: P. Shukla, J. Skea, R. Slade, A. A. Khourdajie, R. van Diemen, D. McCollum, M. Pathak, S. Some, P. Vyas, R. Fradera, M. Belkacemi, A. Hasija, G. Lisboa, S. Luz, J. Malley (Eds.), Climate Change 2022: Mitigation of Climate Change. Contribution of Working Group

- III to the Sixth Assessment Report of the Intergovernmental Panel on Climate Change, Cambridge University Press, Cambridge, UK and New York, NY, USA, 2022, book section 10, pp. 1049–160. doi:https://doi.org/10.1017/9781009157926.
- [11] G.-M. Wu, Z.-Y. Cong, S.-C. Kang, K. Kawamura, P.-Q. Fu, Y.-L. Zhang, X. Wan, S.-P. Gao, B. Liu, Brown carbon in the cryosphere: Current knowledge and perspective, Adv Clim Change Res 7 (1-2) (2016) 82–9. doi:https://doi.org/10.1038/s41561-020-0631-0.
- [12] C. D. Zangmeister, R. You, E. M. Lunny, A. E. Jacobson, M. Okumura, M. R. Zachariah, J. G. Radney, Measured in-situ mass absorption spectra for nine forms of highly-absorbing carbonaceous aerosol, Carbon 136 (2018) 85–93. doi:https://doi.org/10.1016/j.carbon.2018.04.057.
- [13] F. Liu, J. Yon, A. Fuentes, P. Lobo, G. J. Smallwood, J. C. Corbin, Review of recent literature on the light absorption properties of black carbon: Refractive index, mass absorption cross section, and absorption function, Aerosol Sci Technol 54 (1) (2020) 33–51. doi:https://doi.org/10.1080/02786826.2019.1676878.
- [14] H. Michelsen, Probing soot formation, chemical and physical evolution, and oxidation: A review of *in situ* diagnostic techniques and needs, Proc Comb Inst 36 (2017) 717–35. doi:http://dx.doi.org/10.1016/j.proci.2016.08.027.
- [15] P. Parent, C. Laffon, I. Marhaba, D. Ferry, T. Regier, I. Ortega, B. Chazallon, Y. Carpentier, C. Focsa, Nanoscale characterization of aircraft soot: A high-resolution transmission electron microscopy, raman spectroscopy, X-ray photoelectron and near-edge X-ray absorption spectroscopy study, Carbon 101 (2016) 86–100. doi:https://doi.org/10.1016/j.carbon.2016.01.040.
- [16] N. A. Janssen, M. E. Gerlofs-Nijland, T. Lanki, R. O. Salonen, F. Cassee, G. Hoek, P. Fischer, B. Brunekreef, M. Krzyzanowski, Health effects of black carbon, World Health Organization. Regional Office for Europe, 2012.
- [17] M. U. Ali, L. Siyi, B. Yousaf, Q. Abbas, R. Hameed, C. Zheng, X. Kuang, M. H. Wong, Emission sources and full spectrum of health impacts of black carbon associated polycyclic aromatic hydrocarbons (PAHs) in urban environment: A review, Crit Rev Environ Sci Technol 51 (9) (2021) 857–96. doi:https://doi.org/10.1080/10643389.2020.1738854.
- [18] B. Bessagnet, N. Allemand, J.-P. Putaud, F. Couvidat, J.-M. André, D. Simpson, E. Pisoni, B. N. Murphy, P. Thunis, Emissions of carbonaceous particulate matter and ultrafine particles from vehicles A scientific review in a cross-cutting context of air pollution and climate change, Applied Sci 12 (7) (2022) 3623. doi:https://doi.org/10.3390/app12073623.

- [19] H. Zhang, Z. Wang, Advances in the study of black carbon effects on climate, Adv Clim Change Res 2 (1) (2011) 23–30. doi:https://doi.org/10.3724/SP.J.1248.2011.00023.
- [20] T. C. Bond, S. J. Doherty, D. W. Fahey, P. M. Forster, T. Berntsen, B. J. DeAngelo, M. G. Flanner, S. Ghan, B. Kärcher, D. Koch, et al., Bounding the role of black carbon in the climate system: A scientific assessment, J Geophys Res: Atmos 118 (11) (2013) 5380–552. doi:https://doi.org/10.1002/jgrd.50171.
- [21] Q. Lu, C. Liu, D. Zhao, C. Zeng, J. Li, C. Lu, J. Wang, B. Zhu, Atmospheric heating rate due to black carbon aerosols: Uncertainties and impact factors, Atmos Res 240 (2020) 104891. doi:https://doi.org/10.1016/j.atmosres.2020.104891.
- [22] N. Moteki, Climate-relevant properties of black carbon aerosols revealed by in situ measurements: A review, Prog Earth Planet Sci 10 (1) (2023) 12. doi:https://doi.org/10.1186/s40645-023-00544-4.
- [23] M. Kahnert, F. Kanngießer, Modelling optical properties of atmospheric black carbon aerosols, J Quant Spectrosc Radiat Transfer 244 (2020) 106849. doi:https://doi.org/10.1016/j.jqsrt.2020.106849.
- [24] T. C. Bond, R. W. Bergstrom, Light absorption by carbonaceous particles: An investigative review, Aerosol Sci Technol 40 (1) (2006) 27–67. doi:https://doi.org/10.1080/02786820500421521.
- [25] C. Sorensen, Light scattering by fractal aggregates: A review, Aerosol Sci Technol 35 (2) (2001) 648–87. doi:https://doi.org/10.1080/02786820117868.
- [26] J. Yon, C. Rozé, T. Girasole, A. Coppalle, L. Méès, Extension of RDG-FA for scattering prediction of aggregates of soot taking into account interactions of large monomers, Part Part Syst Charac 25 (1) (2008) 54–67. doi:https://doi.org/10.1002/ppsc.200700011.
- [27] J. Yon, F. Liu, A. Bescond, C. Caumont-Prim, C. Rozé, F.-X. Ouf, A. Coppalle, Effects of multiple scattering on radiative properties of soot fractal aggregates, J Quant Spectrosc Radiat Transfer 133 (2014) 374–81. doi:https://doi.org/10.1016/j.jqsrt.2013.08.022.
- [28] M. I. Mishchenko, L. D. Travis, D. W. Mackowski, T-matrix computations of light scattering by nonspherical particles: A review, J Quant Spectrosc Radiat Transfer 55 (5) (1996) 535–75. doi:https://doi.org/10.1016/0022-4073(96)00002-7.
- [29] L. Bi, P. Yang, Accurate simulation of the optical properties of atmospheric ice crystals with the invariant imbedding T-matrix method, J Quant Spectrosc Radiat Transfer 138 (2014) 17–35. doi:https://doi.org/10.1016/j.jqsrt.2014.01.013.

- [30] M. I. Mishchenko, Comprehensive thematic T-matrix reference database: A 2017–2019 update, J Quant Spectrosc Radiat Transfer 242 (2020) 106692. doi:https://doi.org/10.1016/j.jqsrt.2019.106692.
- The discrete-dipole approximation [31] B. Τ. Draine, and itsapplication graphite Astrophys J. 333 (1988)848 - 72.interstellar grains, Part doi:https://doi.org/10.1086/166795.
- [32] B. T. Draine, P. J. Flatau, Discrete-dipole approximation for scattering calculations, J Opt Soc Am A 11 (4) (1994) 1491–99. doi:https://doi.org/10.1364/JOSAA.11.001491.
- [33] F. Moulin, Μ. Devel, S. Picaud, Optical properties of soot nanopar-Spectrosc Transfer 109 (10)(2008)1791-801. Quant Radiat doi:https://doi.org/10.1016/j.jgsrt.2008.01.016.
- [34] R. Langlet, M. Vanacharla, S. Picaud, M. Devel, Bottom-up multi-step approach to study the relations between the structure and the optical properties of carbon soot nanoparticles, J Quant Spectrosc Radiat Transfer 110 (14-16) (2009) 1615–27. doi:https://doi.org/10.1016/j.jqsrt.2009.03.015.
- [35] C. García Fernández, S. Picaud, M. Devel, Calculations of the mass absorption cross sections for carbonaceous nanoparticles modeling soot, J Quant Spectrosc Radiat Transfer 164 (2015) 69–81. doi:https://doi.org/10.1016/j.jqsrt.2015.05.011.
- [36] M. Rérat, J.-C. Rayez, B. Fábián, M. Devel, S. Picaud, A CRYSTAL-based parameterization of carbon atom dynamic polarizabilities to compute optical properties of curved carbonaceous nanostructures, Theor Chem Acc 141 (11) (2022) 65. doi:https://doi.org/10.1007/s00214-022-02926-1.
- [37] N. Brosseau-Habert, F. Miradji, S. Picaud, M. Devel, The reverse-dadi method: Computation of frequency-dependent atomic polarizabilities for carbon and hydrogen atoms in hydrocarbon structures, J Quant Spectrosc Radiat Transfer 329 (2024) 109194. doi:https://doi.org/10.1016/j.jqsrt.2024.109194.
- [38] A. Baldelli, U. Trivanovic, S. N. Rogak, Electron tomography of soot for validation of 2D image processing and observation of new structural features, Aerosol Sci Technol 53 (5) (2019) 575–82. doi:https://doi.org/10.1080/02786826.2019.1578860.
- [39] A. Baldelli, U. Trivanovic, T. A. Sipkens, S. N. Rogak, On determining soot maturity: A review of the role of microscopy-and spectroscopy-based techniques, Chemosphere 252 (2020) 126532. doi:https://doi.org/10.1016/j.chemosphere.2020.126532.

- [40] L. Pascazio, J. W. Martin, K. Bowal, J. Akroyd, M. Kraft, Exploring the internal structure of soot particles using nanoindentation: A reactive molecular dynamics study, Combust Flame 219 (2020) 45–56. doi:https://doi.org/10.1016/j.combustflame.2020.04.029.
- [41] K. Skorupski, J. Mroczka, Effect of the necking phenomenon on the optical properties of soot particles, J Quant Spectrosc Radiat Transfer 141 (2014) 40–8. doi:http://dx.doi.org/10.1016/j.jqsrt.2014.03.001.
- [42] J. Yon, A. Bescond, F. Liu, On the radiative properties of soot aggregates part 1: Necking and overlapping, J Quant Spectrosc Radiat Transfer 162 (2015) 197–206. doi:https://doi.org/10.1016/j.jqsrt.2015.03.027.
- [43] Z. Qin, Q. Zhang, J. Luo, Y. Zhang, Optical properties of soot aggregates with different monomer shapes, Environ Res 214 (2022) 113895. doi:https://doi.org/10.1016/j.envres.2022.113895.
- [44] H. İ. Yazıcı, H. Ertürk, F. Liu, Effect of necking and polydispersity in aggregate and primary particle size on the scattering matrix of soot aggregates, J Aerosol Sci 173 (2023) 106226. doi:https://doi.org/10.1016/j.jaerosci.2023.106226.
- [45] A. Bescond, J. Yon, T. Girasole, C. Jouen, C. Rozé, A. Coppalle, Numerical investigation of the possibility to determine the primary particle size of fractal aggregates by measuring light depolarization, J Quant Spectrosc Radiat Transfer 126 (2013) 130–39. doi:https://doi.org/10.1016/j.jqsrt.2012.10.011.
- [46] X. Wei, Y. Zhu, J. Hu, C. Liu, X. Ge, S. Guo, D. Liu, H. Liao, H. Wang, Recent progress in impacts of mixing state on optical properties of black carbon aerosol, Curr Pollution Rep 6 (2020) 380–98. doi:https://doi.org/10.1007/s40726-020-00158-0.
- [47] P. Minutolo, M. Commodo, A. D'Anna, Optical properties of incipient soot, Proc Comb Inst 39 (1) (2023) 1129–38. doi:https://doi.org/10.1016/j.proci.2022.09.019.
- [48] Y. Wu, L. Zheng, Y. Wu, Z. Wang, Y. Guo, Optical modeling of atmospheric black carbon aerosol ensembles with complex particle morphology, Environ Res Lett 19 (5) (2024) 054017. doi:https://doi.org/10.1088/1748-9326/ad3b21.
- [49] J. Applequist, J. R. Carl, K.-K. Fung, Atom dipole interaction model for molecular polarizability. application to polyatomic molecules and determination of atom polarizabilities, J Am Chem Soc 94 (9) (1972) 2952–60.
- [50] J. Applequist, An atom dipole interaction model for molecular optical properties, Acc Chem Res 10 (3) (1977) 79–85.

- [51] J. Applequist, K. R. Sundberg, M. L. Olson, L. C. Weiss, A normal mode treatment of optical properties of a classical coupled dipole oscillator system with lorentzian band shapes, J Chem Phys 70 (1979) 1240–46. doi:https://doi.org/10.1063/1.437616.
- [52] R. S. Jacobson, A. R. Korte, A. Vertes, J. H. Miller, The molecular composition of soot, Angew Chem 132 (11) (2020) 4514–20. doi:https://doi.org/10.1002/ange.201914115.
- [53] J. Morán, C. Henry, A. Poux, J. Yon, Impact of the maturation process on soot particle aggregation kinetics and morphology, Carbon 182 (2021) 837–46. doi:https://doi.org/10.1016/j.carbon.2021.06.085.
- [54] F. Moulin, S. Picaud, P. N. Hoang, L. Partay, P. Jedlovszky, A grand canonical monte-carlo simulation study of water adsorption on a model soot particle, Mol Sim 32 (7) (2006) 487–93. doi:https://doi.org/10.1080/08927020600622048.
- [55] G. Hantal, S. Picaud, P. N. Hoang, V. P. Voloshin, N. N. Medvedev, P. Jedlovszky, Water adsorption isotherms on porous onionlike carbonaceous particles. simulations with the grand canonical monte carlo method, J Chem Phys 133 (14) (2010). doi:https://doi.org/10.1063/1.3496466.
- [56] B. Gigone, A. E. Karataş, Ö. L. Gülder, Soot aggregate morphology in coflow laminar ethylene diffusion flames at elevated pressures, Proceedings of the Combustion Institute 37 (1) (2019) 841–848. doi:https://doi.org/10.1016/j.proci.2018.06.103.
- [57] U. Trivanovic, S. E. Pratsinis, Opinion: Eliminating aircraft soot emissions, Aerosol Research 2 (2024) 207–223. doi:https://doi.org/10.5194/ar-2-207-2024.
- [58] A. P. Thompson, H. M. Aktulga, R. Berger, D. S. Bolintineanu, W. M. Brown, P. S. C. et al., LAMMPS A flexible simulation tool for particle-based materials modeling at the atomic, meso, and continuum scales, Comp. Phys. Comm. 271 (2022) 108171. doi:10.1016/j.cpc.2021.108171.
- [59] S. J. Stuart, A. B. Tutein, J. A. Harrison, A reactive potential for hydrocarbons with intermolecular interactions, J Chem Phys 112 (14) (2000) 6472–86. doi:https://doi.org/10.1063/1.481208.
- [60] B. Draine, H. M. Lee, Optical properties of interstellar graphite and silicate grains, Astrophys J 285 (1984) 89–108. doi:https://doi.org/10.1063/1.481208.
- [61] P. Senet, L. Henrard, P. Lambin, A. Lucas, H. Kuzmany, J. Fink, M. Mehring, S. Roth, A one parameter model of the UV spectra of carbon, Proceedings of the international winterschool on electronic properties of novel materials. Progress in fullerene research (1994) 393–96doi:https://doi.org/10.1142/9789814533850.

- [62] J. U. Andersen. Ε. Bonderup. Classical dielectric models of heat Phys J D 11 (2000)and estimation radiation, Eur 413 - 34. doi:https://doi.org/10.1007/s100530070070.
- [63] T. L. Farias, Ü. Ö. Köylü, M. d. G. Carvalho, Range of validity of the Rayleigh–Debye–Gans theory for optics of fractal aggregates, Applied optics 35 (33) (1996) 6560–6567. doi:https://doi.org/10.1364/AO.35.006560.
- [64] Y. Zhao, L. Ma, Applicable range of the Rayleigh–Debye–Gans theory for calculating the scattering matrix of soot aggregates, Appl Opt 48 (3) (2009) 591–97. doi:https://doi.org/10.1364/AO.48.000591.
- [65] C. M. Sorensen, J. Yon, F. Liu, J. Maughan, W. R. Heinson, M. J. Berg, Light scattering and absorption by fractal aggregates including soot, J Quant Spectrosc Radiat Transfer 217 (2018) 459–73. doi:https://doi.org/10.1016/j.jqsrt.2018.05.016.
- [66] C. Argentin, M. J. Berg, M. Mazur, R. Ceolato, J. Yon, Assessing the limits of Rayleigh—Debye—Gans theory: Phasor analysis of a bisphere, J Quant Spectrosc Radiat Transfer 264 (2021) 107550. doi:https://doi.org/10.1016/j.jqsrt.2021.107550.
- [67] C. Argentin, M. J. Berg, M. Mazur, R. Ceolato, A. Poux, J. Yon, A semi-empirical correction for the Rayleigh–Debye–Gans approximation for fractal aggregates based on phasor analysis: Application to soot particles, J Quant Spectrosc Radiat Transfer 283 (2022) 108143. doi:https://doi.org/10.1016/j.jqsrt.2022.108143.
- [68] A. Coderre, K. Thomson, D. Snelling, M. Johnson, Spectrally resolved light absorption properties of cooled soot from a methane flame, Applied Physics B 104 (2011) 175–188. doi:10.1007/s00340-011-4448-9.
- [69] E. Sohmen, J. Fink, W. Krätschmer, Electron energy-loss spectroscopy studies on C_{60} and C_{70} fullerite, Z Phys B Cond Mat 86 (1) (1992) 87–92. doi:https://doi.org/10.1007/BF01323552.
- [70] C. Liu, X. Xu, Y. Yin, M. Schnaiter, Y. L. Yung, Black carbon aggregates: A database for optical properties, J Quant Spectrosc Radiat Transfer 222 (2019) 170– 79. doi:https://doi.org/10.1016/j.jqsrt.2018.10.021.
- [71] D. W. Mackowski, M. I. Mishchenko, A multiple sphere T-matrix fortran code for use on parallel computer clusters, J Quant Spectrosc Radiat Transfer 112 (13) (2011) 2182– 2192. doi:https://doi.org/10.1016/j.jqsrt.2011.02.019.
- [72] D. W. Mackowski, The extension of the multiple sphere T-matrix code to include multiple plane boundaries and 2-D periodic systems, J Quant Spectrosc Radiat Transfer 290 (2022) 108292. doi:https://doi.org/10.1016/j.jqsrt.2022.108292.